Size quantization effects in atomic level broadening near thin metallic films

U. Thumm
J.R. Macdonald Laboratory, Department of Physics, Kansas State University, Manhattan, Kansas 66506-2601 and Institute for Theoretical Atomic and Molecular Physics, Harvard-Smithsonian Center for Astrophysics, 60 Garden Street, Cambridge, Massachusetts 02138

P. Kürpick*
J.R. Macdonald Laboratory, Department of Physics, Kansas State University, Manhattan, Kansas 66506-2601

U. Wille
Bereich Theoretische Physik, Hahn-Meitner-Institut Berlin, Glienicker Strasse 100, D-14109 Berlin, Germany
(Received 16 February 1999)

The broadening of atomic levels near thin metallic films is studied theoretically within the fixed-atom approximation. First-order level widths are calculated by using a Jennings-type jellium potential to describe the electronic states of the film, and hydrogenic wave functions in parabolic (Stark) representation for the atomic orbitals. In the parabolic representation, hybridization effects due to the long-range image-charge interactions are taken into account. Size quantization in the growth direction of the film gives rise to characteristic structures in level widths, atomic occupation probabilities, and transition distances as a function of the film thickness. Details of this structure depend on the orientation of the Stark orbitals with respect to the film and can be related to the dependence of transition matrix elements on the active electron's wave vector component parallel to the surface for the case of a semi-infinite metal. The large variation of the calculated transition distances with the film thickness may result in observable effects in atomic interactions with thin films.

I. INTRODUCTION

Over the past decades, electronic processes that occur when slowly moving atoms and ions interact with solid surfaces have been a subject of intense study. A large number of investigations have dealt with the interaction of neutral atoms and of ions in low charge states with clean surfaces of semi-infinite metal targets. In recent years, the scope of ion-surface studies has been considerably extended through the use of multiply charged projectile ions (see Ref. 1 and references cited therein), in conjunction with metallic targets as well as with semi-conducting and insulating targets.[2,3] Further, the effect of adsorbates and thin dielectric films covering metal surfaces has been examined.[4–6]

The use of thin metallic films, instead of semi-infinite metal targets, in the study of electronic processes in ion-surface interactions has been suggested recently by Borisov and Winter.[7,8] A thin metallic film may be formed by depositing a metal overlayer on a dielectric substrate with the band gap extending over the conduction band of the metal. In this kind of structure, the electronic motion in the growth direction (z axis) is confined between the metal-substrate interface and the metal-vacuum interface, whereas the two-dimensional motion in the film plane is supposed to be free. The confinement in z direction gives rise to quantization (''size quantization''), with discrete eigenvalues of the associated energy. The similarity of this situation to that encountered in two-dimensional quantum well structures formed by semiconductors of different chemical composition[9] is obvious.

The size quantization in thin-metallic films allows, through the variation of the film thickness, the density of metal states to be varied and hence the transition rates for electron transfer out of, and into, the metal to be influenced. Details of the discrete energy spectrum of the film are expected to give rise to specific resonance and threshold phenomena. In principle, studies involving thin films may therefore yield insight into structural properties of the films and may furnish a more sensitive test of the ion-surface interaction than do studies with semi-infinite targets. Up to now, the details of electronic processes in ion interactions with thin metallic films have been treated only theoretically[7,8] (see also Ref. 10), and sizeable deviations from calculations for the semi-infinite case were obtained for the neutralization of Na^+ ions and for the formation of H^- ions near thin Al(111) films. We mention that the grazing-incidence ion scattering technique has recently been applied[11,12] to study experimentally the growth and morphology of thin Mn films (thickness $\leqslant 12$ monolayers) on Fe(100) substrates. While ion scattering is used here as an analytic tool, a detailed theoretical understanding of the basic electronic processes occurring in ion-film interactions will be important also in this case.

In the present paper, we study the broadening of *hydrogenic* levels near thin-metallic films by evaluating first-order level widths (or, equivalently, transition rates for resonant transfer of electrons or holes between atom and film), atomic occupation probabilities, and transition distances for resonance ionization of atoms and resonance neutralization of ions. The case of hydrogenic levels is of particular interest as it constitutes the prototype case for the treatment of the interaction of highly charged ions and Rydberg atoms with thin films. The self-energy method[13] that has been successfully applied in the *nonperturbative* calculation of shifts and widths of hydrogenic levels for semi-infinite targets[14,15] ap-

pears to be equally well suited for the case of thin-metallic films. However, it becomes apparent from our results below that in the thin-film case already the first-order widths, which are essentially equal to the imaginary parts of the diagonal elements of the self-energy matrix, display a variety of novel features whose thorough analysis is advisable, if not indispensable, before a full self-energy calculation is performed.

In the next section, we outline the theoretical framework for our calculations. Section III contains a heuristic discussion of qualitative features of the level widths, followed by the presentation of numerically calculated widths. Atomic occupation probabilities and transition distances are presented in Sec. IV. A comprehensive discussion of our results, including a brief examination of the possibility to observe features revealed by our calculations in suitably devised experiments, is given in Sec. V. Finally, Sec. VI contains a summary of the paper as well as some concluding remarks.

II. THEORY

We adopt the jellium model for the metallic film of thickness L and construct the unperturbed electronic potential $V_{\rm film}(z)$ by using the analytic electron-surface potential of Jennings *et al.*[16] (with one and the same set of parameters) to describe the interfaces on either side of the film.[7,8] The Jennings potential constitutes an analytic fit to the results of density functional calculations. Taking $z=0$ to correspond to the midpoint of the film, we have

$$V_{\rm film}(z)=\begin{cases} -V_0/\{A\exp[B(|z|-L/2)]+1\}, & |z|\leq L/2 \\ -\{1-\exp[-\eta(|z|-L/2)]\}/[4(|z|-L/2)], & |z|>L/2 \end{cases} \tag{1}$$

($A=4V_0/\eta-1$, $B=2V_0/A$). In our calculations, we use parameter values appropriate to the description of Al(111): $V_0=0.58581$ a.u., $\eta=1$ a.u. Note that for $|z|\to\infty$, the Jennings potential merges in the classical self-image potential of the electron (the image reference plane is assumed to coincide with the jellium edges $|z|=L/2$).

The potential (1) is symmetric with respect to coordinate inversion, $V_{\rm film}(-z)=V_{\rm film}(z)$, so that the asymmetry caused by the presence of a substrate on one side of the film cannot be taken into account in our calculations. However, except for very small film thickness, the substrate should have very little effect on the atomic level widths, which are mainly determined by the overlap of film wave function and atomic wave function in the spatial region between film and atom. Owing to the symmetry of $V_{\rm film}(z)$, the bound-state eigenfunctions $\phi_i(z)$ (with labels $i=1,2\ldots$ arranged in order of increasing energy eigenvalue ϵ_i) of the z-dependent part of the film Hamiltonian are simultaneously eigenfunctions of the parity operator, with eigenvalue $(-1)^{i-1}$. The total film wave functions $\phi_{\vec{k}_\parallel i}(\vec{r})$ are written as

$$\phi_{\vec{k}_\parallel i}(\vec{r})=\exp(i\vec{k}_\parallel\cdot\vec{r}_\parallel)\,\phi_i(z), \tag{2}$$

where $\vec{k}_\parallel$ and $\vec{r}_\parallel$ are the components of wave vector and position vector, respectively, in the film plane. Assuming unit normalization for the discrete states ϕ_i, the orthonormality relation for the states $\phi_{\vec{k}_\parallel i}$ reads

$$\langle\phi_{\vec{k}_\parallel i}|\phi_{\vec{k}'_\parallel i'}\rangle=(2\pi)^2\delta^{(2)}(\vec{k}_\parallel-\vec{k}'_\parallel)\,\delta_{ii'}, \tag{3}$$

and the density of states (for fixed projection of the electron spin) associated with the motion in the film plane, $\rho(\vec{k}_\parallel)$, is accordingly equal to $(2\pi)^{-2}$. The energies associated with the states $\phi_{\vec{k}_\parallel i}$ are

$$\epsilon_{k_\parallel i}=\frac{1}{2}k_\parallel^2+\epsilon_i \tag{4}$$

(we use atomic units throughout).

For the purpose of illustration, we show in Fig. 1 the potential (1) for $z\geq 0$ for an Al film of thickness $L=20$ a.u., together with the energies ϵ_i of the lowest 13 bound states, plotted against the index i. Also shown are the (normalized) wave functions $\phi_i(z)$ for $i=1,\ldots,4$ and $i=10,\ldots,13$ in the range $z\geq 0$ [for $z<0$, the functions are obtained by symmetric or asymmetric continuation, depending on whether the parity $(-1)^{i-1}$ is equal to $+1$ or -1). The spectrum of the eigenvalues ϵ_i is characterized by an accumulation point at zero energy, which is related to the long-range behavior of the electronic self-image potential included in the potential (1) (see also Fig. 2 and the discussion below). Correspondingly, the wave functions for the highest eigenvalues extend far beyond the jellium edge into the vacuum.

For the hydrogenic wave functions of the unperturbed

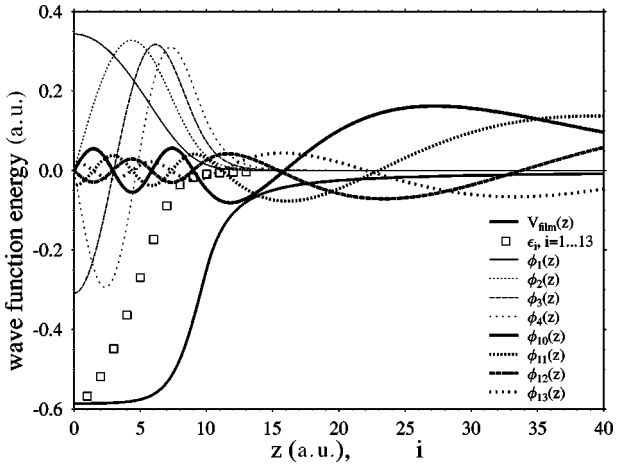

FIG. 1. The potential $V_{\rm film}(z)$ [cf. Eq. (1)] for an Al(111) film of thickness $L=20$ a.u., its lowest energy levels ϵ_i (plotted versus the index i), and selected (normalized) bound-state wave functions $\phi_i(z)$. Potential and wave functions in the range $z<0$ are obtained by symmetric or antisymmetric continuation (see text).

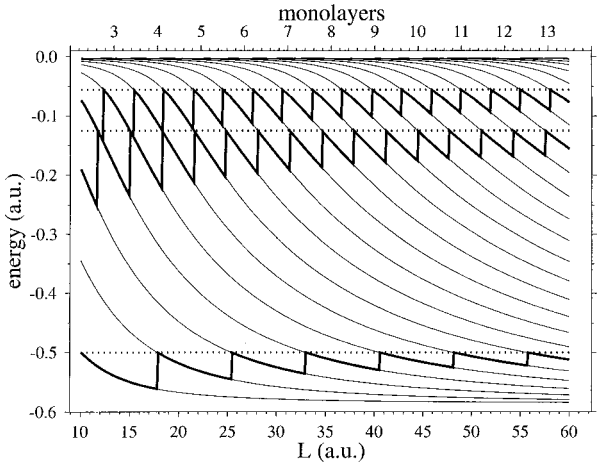

FIG. 2. Energy levels ϵ_i of an Al(111) film described by the potential (1), plotted as a function of film thickness L. The dotted horizontal lines indicate the unperturbed levels of the hydrogen atom for $n=1,2,3$. The heavy solid lines emphasize those pieces of the film level curves that belong to the first film level *below* a given hydrogen level.

atomic system, we adopt the parabolic (Stark) representation $\psi_{nkm}(\vec{r})$, with principal quantum number n, ''electric'' quantum number k, and magnetic quantum number m. Using this representation, we take into account, to some extent, the hybridization of the atomic orbitals induced by the long-range image charge interactions in the atom-metal system.[17] For the semi-infinite case, first-order widths have been calculated for hydrogenic levels in parabolic representation *without* explicit inclusion of the image charge interactions. These widths were found to be in good overall agreement with widths obtained from calculations within the nonperturbative coupled-angular-mode method,[18,19] in which both the electronic self-image potential and the image potential induced by the atomic core were explicitly included.

In fixed-atom approximation, the first-order width $\Gamma_{nkm}(D)$ of a hydrogenic level with quantum numbers n,k,m, associated with an atom located at a distance D from the adjacent jellium edge of the metallic film, is given by

$$\Gamma_{nkm}(D)=2\pi\sum_i \int d\vec{k}_\parallel \rho(\vec{k}_\parallel)\,|W_{nkm,\vec{k}_\parallel i}(D)|^2\,\delta(\epsilon_n-\epsilon_{k_\parallel i}), \tag{5}$$

where $\epsilon_n=-Z^2/2n^2$ (Z=effective core charge) is the unperturbed energy of the hydrogenic level. Note that we disregard the atomic level shift which, to lowest order, is given by $(2Z-1)/4D$. For atom-film distances close to, or beyond, the classical threshold distance, level widths are only weakly affected by the rather small level shifts. At the low perpendicular velocities typical for current grazing-incidence experiments with Rydberg atoms and highly charged ions as projectiles and semi-infinite targets, transitions are most likely to occur in this range of distances. Therefore, the inclusion of the level shift would tend to slightly shift and blur the calculated structure in the L dependence of the transition distances (cf. Sec. IV) but would not alter our conclusions (cf. Sec. V).

The transition-matrix element $W_{nkm,\vec{k}_\parallel i}(D)$ is written as

$$W_{nkm,\vec{k}_\parallel i}(D)=\langle\psi_{nkm}(D)|\,V_C^{>}(D)\,|\phi_{\vec{k}_\parallel i}\rangle \tag{6}$$

with the perturbing potential

$$V_C^{>}=V_C\Theta(z-L/2), \tag{7}$$

where V_C is the Coulomb potential of the atomic core, and $\Theta(z)$ is the unit step function (the z axis is directed from the midpoint of the film towards the atom). The core *image* potential has been neglected in the potentials defining the unperturbed atomic and film states and in the perturbing potential (7).[14,20] However, its effect on level hybridization is partly taken into account in the atomic states through the use of hydrogenic wave functions in parabolic representation.[17] The explicit inclusion of the full core image potential in our calculations would entail a greatly increased numerical effort. The self-image potential of the electron, on the other hand, is included in the unperturbed film potential. Therefore, when using the parabolic representation for the hydrogenic wave functions, parts of the self-image potential are taken into account twice. Without exhaustive analysis, it appears hard to decide whether it is more accurate in general to count parts of the self-image potential twice or to disregard certain parts of it. However, in the specific results presented below, the explicit inclusion of the self-image potential in $V_{\rm film}(z)$ is found to have little effect.

The specific form of the potential (7) reflects our assumption that the core potential is completely screened inside the film and the substrate. Furthermore, our choice for the perturbing potential in Eq. (6) corresponds to the ''post form'' of the transition-matrix element, which represents one of two admissible alternatives (strictly equivalent in the resonant case) for writing the matrix element.[20,21] Assuming the underlying total electronic potential V in the atom-film system to have the form $V=V_{\rm film}+V_C^{>}$, one obtains the perturbing potential $V_{\rm pert}$ of the ''post'' form by subtracting $V_{\rm film}$ from V, $V_{\rm pert}=V-V_{\rm film}=V_C^{>}$. We choose the ''post'' form of the transition matrix element since it is slightly easier to handle in the numerical calculations.

Resolving the δ function in Eq. (5) and exploiting the azimuthal symmetry of the transition-matrix element in $\vec{k}$ space, we can express the level width as

$$\Gamma_{nkm}(D)=\sum_i |W_{nkm,k_\parallel^{(i)}}(D)|^2\Theta(\epsilon_n-\epsilon_i), \tag{8}$$

where

$$k_\parallel^{(i)}=\sqrt{2(\epsilon_n-\epsilon_i)} \tag{9}$$

(when used as a label in $W_{nkm,k_\parallel^{(i)}}$, $k_\parallel^{(i)}$ is assumed to refer to the dependence of the matrix element on the wave function ϕ_i). The width thus appears as a sum over a finite number of terms corresponding to transitions of electrons or holes (depending on the position of the atomic level ϵ_n relative to the Fermi level ϵ_F of the film; note that ϵ_F depends on the film thickness L[8]) into film states with energy $\epsilon_i\leqslant\epsilon_n$ in the growth direction and (real) wave vector $k_\parallel^{(i)}$ of the free in-plane motion, such that the resonance condition for the total energy, $\epsilon_{k_\parallel i}=\epsilon_n$, is fulfilled.

For the general (resonant or non resonant) case, the evaluation of the transition-matrix elements $W_{nkm,\vec{k}_\parallel i}$ is easily ac-

complished by expressing them in terms of the matrix elements $W_{nlm,\vec{k}_\parallel i}$ corresponding to the spherical representation of the hydrogenic wave functions (l is the orbital angular momentum),[22]

$$W_{nkm,\vec{k}_\parallel i}=\sum_{l=m}^{n-1} c_{n,k}^{l,m} W_{nlm,\vec{k}_\parallel i}, \tag{10}$$

where

$$c_{n,k}^{l,m}\equiv\left(\begin{matrix}(n-1)/2 & (n-1)/2\\ (m+k)/2 & (m-k)/2\end{matrix}\middle|\begin{matrix}l\\ m\end{matrix}\right) \tag{11}$$

is a Clebsch-Gordan coefficient. In the matrix elements $W_{nlm,\vec{k}_\parallel i}$, the two-dimensional integration over the coordinates in the film plane can be performed in closed form, using the technique of Ref. 23. In the remaining one-dimensional integral, the film wave function is folded with an atomic form factor $A_{nlm,\vec{k}_\parallel}$ that comprises the properties of the atomic wave function and of the perturbing Coulomb potential (see Appendix A for details). Exploiting symmetry properties of the form factor, we can write

$$W_{nlm,\vec{k}_\parallel i}(D)=\int_0^\infty d\zeta\{\phi_i(\zeta+\Delta)+(-1)^{l+m}\phi_i(-\zeta+\Delta) \times\Theta(-\zeta+D)\}A_{nlm,\vec{k}_\parallel}(\zeta), \tag{12}$$

where $\zeta=z-\Delta$ and $\Delta\equiv L/2+D$; the step function $\Theta(-\zeta+D)$ reflects the cutoff in the potential (7). A simple analytic expression for $A_{nlm,\vec{k}_\parallel}$ exists for arbitrary quantum numbers n,l,m. The numerical effort required to evaluate the transition-matrix elements thus consists (i) in generating the wave functions $\phi_i(z)$ for the potential (1), and (ii) in performing the ζ-integration in the integral (12).

Assuming the atom to approach the thin film along a classical trajectory, we can use the widths calculated from Eq. (8) to evaluate occupation probabilities for atomic states within the rate equation method. As we disregard level shifts, a given atomic level is above or below the Fermi level ϵ_F throughout. For an electron or hole occupying at $D=\infty$ the atomic state ψ_{nkm} with unit probability, the probability to occupy this state at distance D is then given by[24]

$$P_{nkm}(D)=\exp\left\{-\frac{1}{v_z}\int_D^\infty dD'\Gamma_{nkm}(D')\right\}, \tag{13}$$

provided the atom moves with constant velocity along a straight-line trajectory (v_z is the absolute magnitude of the z-component of the velocity). If the probabilities $P_{nkm}(D)$ drop from unity to zero in a sufficiently narrow D range, one may determine transition distances D_{nkm} (i.e., distances for resonance ionization or neutralization, depending on whether $\epsilon_n>\epsilon_F$ or $\epsilon_n<\epsilon_F$) by solving the equation $P_{nkm}(D_{nkm})=0.5$.

We note that the inclusion of atomic level shifts would entail distance-dependent Fermi factors in the rate equations for the occupation probabilities. In Sec. V, we discuss qualitatively the interaction of very low-velocity Rydberg atoms and highly charged ions with thin films. For highly charged ions, electronic transitions into Rydberg levels occur at very large atom-film distances. For both highly charged ions and Rydberg atoms, the large transition distances result in small level shifts and relevant Fermi factors that are essentially equal to unity. Therefore, for the purpose of our discussion, Eq. (13) appears to be a sufficiently good approximation.

III. ATOMIC LEVEL WIDTHS

As the thickness L is the principal parameter characterizing the film properties, we confine ourselves in this section to the study of the L dependence of the level widths at fixed atom-film distance D. The D dependence of the widths at fixed L will be considered in Sec. IV in conjunction with the calculation of atomic occupation probabilities and transition distances. Before turning to the numerical calculations, we discuss the L dependence of the level widths in a heuristic way in order to facilitate the qualitative understanding of the complex features observed in the numerical results.

A. Heuristic discussion

From Eq. (8), it is evident that the L dependence of the widths is decisively influenced by the L dependence of the energies ϵ_i. In Fig. 2, we show the latter dependence for a thin Al(111) film over an L range extending approximately from 2 to 14 monolayers [based on the bulk lattice constant $a=7.7$ a.u., the spacing between monolayers, i.e. the distance between (111) planes in Al (111), is $a/\sqrt{3}=4.4$ a.u.]. Also shown are horizontal lines indicating the unperturbed energies of the hydrogen atom ($Z=1$) for $n=1,2,3$. The film levels decrease monotonically with increasing L. With decreasing energy, i.e., as the levels move towards the bottom of the film potential well, the effect of the self-image potential is found to die away rapidly. Its inclusion is expected to be irrelevant for the film states sampled in the present study, which is confined to hydrogen levels with $n\leqslant 3$ and hence to film levels below the $n=3$ level.

According to Eq. (8), the point of intersection L_i of a film level curve $\epsilon_i(L)$ with the horizontal line for a given atomic level ϵ_n defines the threshold for transitions into the film state labeled i. When L increases from L_i, the resonant in-plane wave vector $k_\parallel^{(i)}$ rises from zero upwards [cf. Eq. (9)], while the wave vectors $k_\parallel^{(i-1)}, k_\parallel^{(i-2)}, \ldots$ associated with the levels $\epsilon_{i-1}(L), \epsilon_{i-2}(L), \ldots$ rise from progressively larger (positive) values at L_i. A continuous variation of L thus induces, via the variation of the energies $\epsilon_i(L), \epsilon_{i-1}(L), \epsilon_{i-2}(L), \ldots$, a continuous variation of $k_\parallel$ in the corresponding resonant transition matrix elements contributing to the level width Γ_{nkm} for a thin film. By comparison, in the case of resonant transitions into a semi-infinite metal, a continuous variation of $k_\parallel=\sqrt{2(\epsilon_n-\epsilon_z)}$ can be directly induced by varying the energy associated with the electronic motion in z direction, ϵ_z, which is a continuous eigenvalue. Hence, provided the L dependence of the energies ϵ_i is sufficiently smooth (cf. Fig. 2), the L-dependence of the transition-matrix elements and level widths for thin films is expected to image the $k_\parallel$ dependence of the transition matrix elements for the semi-infinite case. For exhibiting the latter dependence, we have calculated resonant transition-

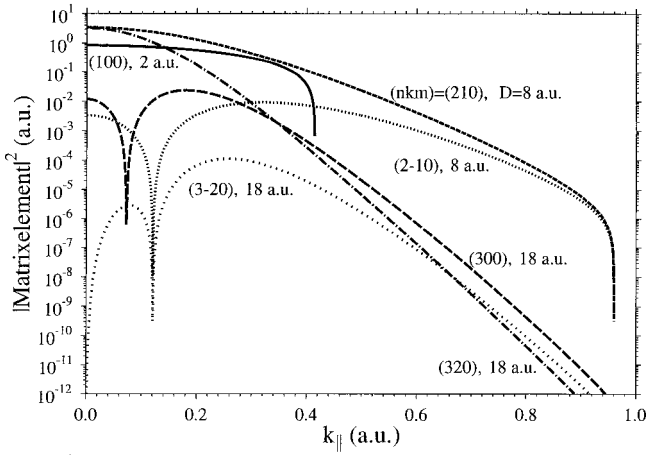

FIG. 3. Squared resonant transition matrix elements for a hydrogen atom in front of a semi-infinite Al(111) target (Ref. 23) plotted as a function of the wave vector component $k_\parallel$ parallel to the surface, for the indicated values of the quantum numbers n,k,m. The distances D are equal to the classical threshold distances $D_n=2n^2$ for the superposition of a steplike jellium potential and the potential (7).

matrix elements for a steplike jellium potential and the perturbing potential (7).[23] In Fig. 3, matrix elements are shown for the $m=0$ levels of the $n=1,2,3$ manifolds of a hydrogen atom located respectively at the distance $D_n=2n^2$ in front of an Al(111) surface. The classical threshold distances D_n are obtained for the superposition of the step potential and the potential (7) and correspond to ion-surface distances at which electronic transitions are most likely to occur.[20,23]

The curves in Fig. 3 for the maximum value $k_{\max}=n-1$ of the electric quantum number k within each n manifold are seen to decrease monotonically with $k_\parallel$. For these cases, the L dependence of the level widths for the thin film is thus expected to display a discontinuous rise at the thresholds L_i and a monotonic decrease between L_i and L_{i+1}, independent of the value of i. Moreover, the dominant contribution to the atomic level width will arise from the first film level below the atomic level. The qualitative behavior of the level widths as a function of L should resemble the saw-tooth pattern in the level diagram of Fig. 2, which has been obtained by emphasizing, for each n, those pieces of the level curves that belong to the first film level below a given atomic level.

The structure in the curves of Fig. 3 for electric quantum numbers $k<k_{\max}$ suggests a more complex L dependence of the corresponding level widths. Considering, e.g., the case $(n,k,m)=(3,-2,0)$, we expect the zero at $k_\parallel=0$ of the matrix element for the semi-infinite case to find its counterpart in a zero at L_i of the matrix element involving the first film level below the $n=3$ level. The second film level at L_i, however, corresponds to $k_\parallel\approx 0.25...0$ .4 a.u. when L_i is in the L-range plotted in Fig. 2. In this $k_\parallel$ range, the curve in Fig. 3 exhibits a broad maximum. Thus the atomic level width at L_i will receive its dominant contribution from the second film level. When L varies between L_i and L_{i+1}, detailed structure resulting from the superposition of contributions of the first, second, and possibly third film level below the atomic level may be anticipated. A weak dependence of the detailed structure on the location of the interval $[L_i,L_{i+1}]$ should arise from the change of the slope of the film level curves with L. Disregarding this dependence, the pattern of the detailed structure for a given atomic level will be periodically repeated, with the period $\Delta L=L_{i+1}-L_i$ being virtually independent of i (cf. Fig. 2).

B. Numerical results

Having developed a qualitative idea of how the L dependence of the atomic level widths looks like, we now turn to the explicit calculation of level widths for the hydrogen atom. In view of the expected features, it is appropriate to evaluate the periodic ''gross structure'' of the L-dependence over the full L range of Fig. 2 and restrict the calculation of the detailed structure to selected periodicity intervals $[L_i,L_{i+1}]$.

In order to exhibit the gross structure of the L dependence, we have calculated level widths for the distances D_n $(n=1,2,3)$ of Fig. 3 at the positions $L_i-\lambda$ and $L_i+\lambda$ for all L_i, i.e., in the vicinity of all discontinuities in the saw-tooth pattern of Fig. 2, in the interval 10 a.u. $\leqslant L\leqslant$60 a.u. (the value of the parameter λ is of the order of 0.01 a.u.). The curves resulting from smoothly interpolating the widths (in a log-lin plot) between $L_i+\lambda$ and $L_{i+1}-\lambda$ are shown in Fig. 4. The detailed structure for the hydrogen $n=1,2,3$ manifolds, obtained from calculations on a very dense L grid covering the periodicity intervals

$$I_1=[17.8\ \text{a.u.},\ 25.4\ \text{a.u.}],$$

$$I_2=[21.5\ \text{a.u.},\ 24.8\ \text{a.u.}], \tag{14}$$

$$I_3=[21.5\ \text{a.u.},\ 24.5\ \text{a.u.}],$$

respectively, is displayed in Fig. 5. In addition to the total level widths, the contributions arising from different film states are shown in this figure. The results of Fig. 5 fully confirm the qualitative picture developed in Sec. III A. This pertains, in particular, to the number and relative position of the extrema in the curves for electric quantum numbers $k<k_{\max}$. Combining the results of Figs. 4 and 5, the following picture emerges for the L-dependence of the atomic level widths.

If $k=k_{\max}$, the curves for the level widths in Fig. 5 exhibit near-exponential behavior in the selected intervals (14). The interpolated curves of Fig. 4 thus provide a good representation of the detailed shape that would be revealed by a calculation on a very dense grid over the full L range. If $k<k_{\max}$, modulations show up in the curves of Fig. 5, with the maximum (minimum) in general not coinciding with L_i. In this case, the interpolated curves of Fig. 4 may be interpreted as average curves. If we would replace the true curves in Fig. 5 with exponentials fitted to the true curves, e.g., at L_i, in such a way that the integral over true and fit curve agree, the slopes of the exponentials would in general deviate from those of the corresponding exponentials in Fig. 4. However, from the examples shown, it appears that the discrepancies are fairly small.

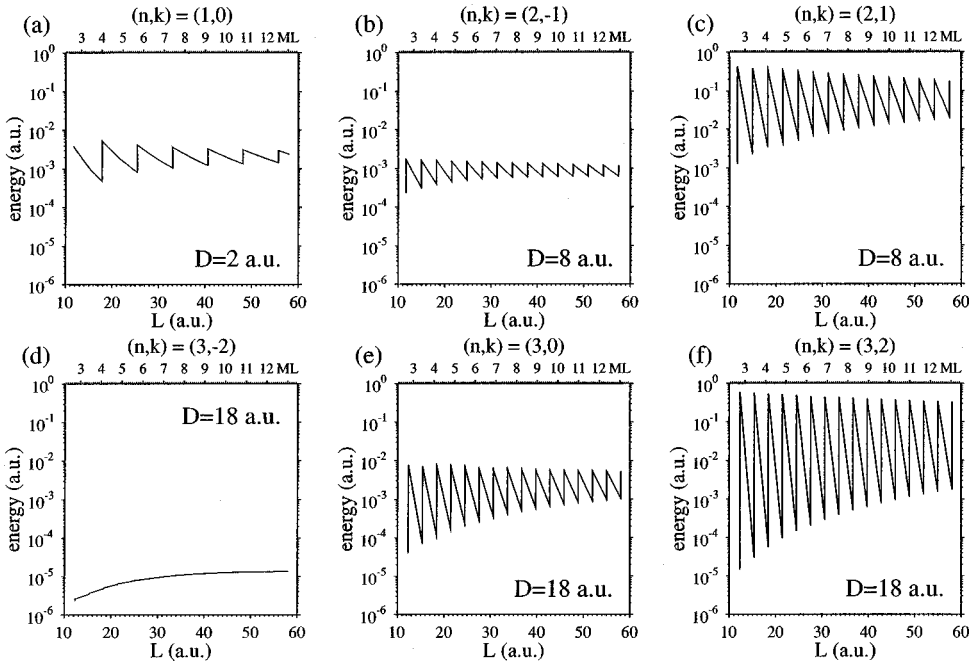

FIG. 4. Gross structure of the L dependence of the level widths Γ_{nkm} [cf. Eq. (8)] for a hydrogen atom located at the distances $D_n = 2n^2$ in front of an Al(111) film, for $m=0$ and the indicated values of the quantum numbers n,k. For further explanation, see text.

IV. OCCUPATION PROBABILITIES AND TRANSITION DISTANCES

According to Eq. (13), the occupation probabilities $P_{nkm}(D)$ are essentially determined by the integral $\int_D^\infty dD' \Gamma_{nkm}(D')$. Hence, a brief discussion of the D-dependence of the level widths Γ_{nkm} is appropriate here. As mentioned earlier and as mandated by the Pauli exclusion principle, the following results for $n=1$ relate to the decay of a hydrogen K-shell *hole* into the film, whereas for $n \geqslant 2$ all occupation probabilities and transition distances describe the transfer of a hydrogen *electron* into the film.

In Fig. 6, the D dependence of Γ_{nkm} is shown for the hydrogen $n=1,2,3$ manifolds with $m=0$ for selected L values inside the intervals (14) and, in addition, for one L-value just below each interval. Therefore, when going from the smallest L to the second smallest, one crosses the thresholds associated with the points of intersection of the film level curves with the atomic levels (cf. Fig. 2). Drastic threshold effects are observed in the curves of Fig. 6 for $k=k_{\max}$. Independent of D, the widths increase by one order of magnitude ($n=1$) to four orders of magnitude ($n=3$) [except for the small-D range for $(n,k)=(3,2)$] when the thresholds are crossed. Above the thresholds, a rapid monotonic (D independent) decrease of the widths with L is found. Note that in the plots (a), (c), and (f) of Fig. 5, these effects are exhibited for the specific distances $D=D_n$. With decreasing electric quantum number k, the threshold effects in the width curves of Fig. 6 become progressively blurred.

The D dependence of the occupation probabilities P_{nkm} $(n=1,2,3; m=0)$ is shown in Fig. 7 for v_z

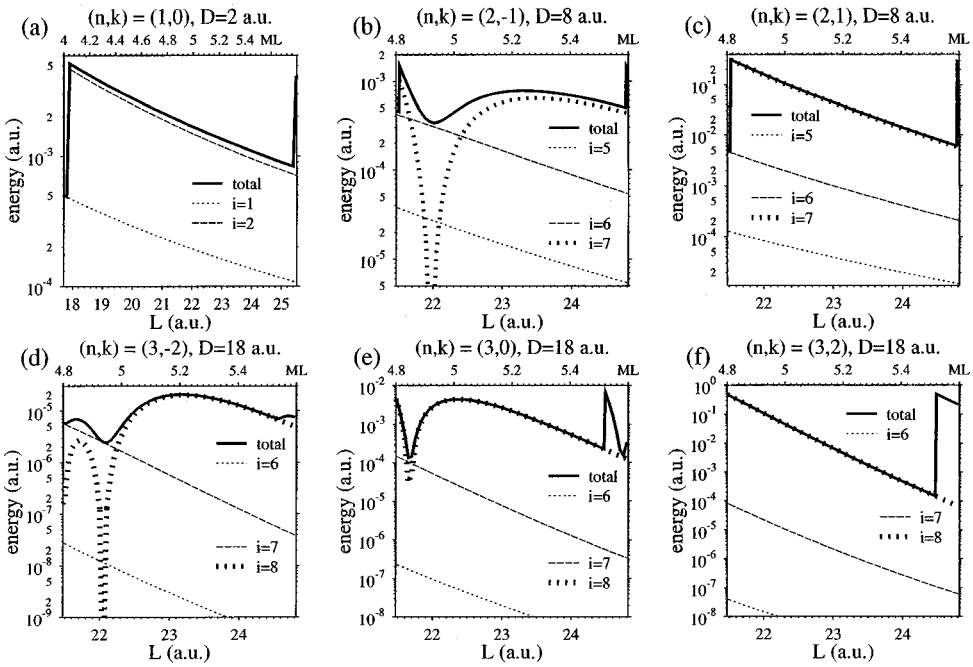

FIG. 5. Detailed structure of the L dependence of the level widths for the case of Fig. 4, evaluated over the periodicity intervals I_n defined in Eq. (14). Also shown are the contributions to the widths from the film states lying energetically closest below the atomic level (cf. Fig. 2).

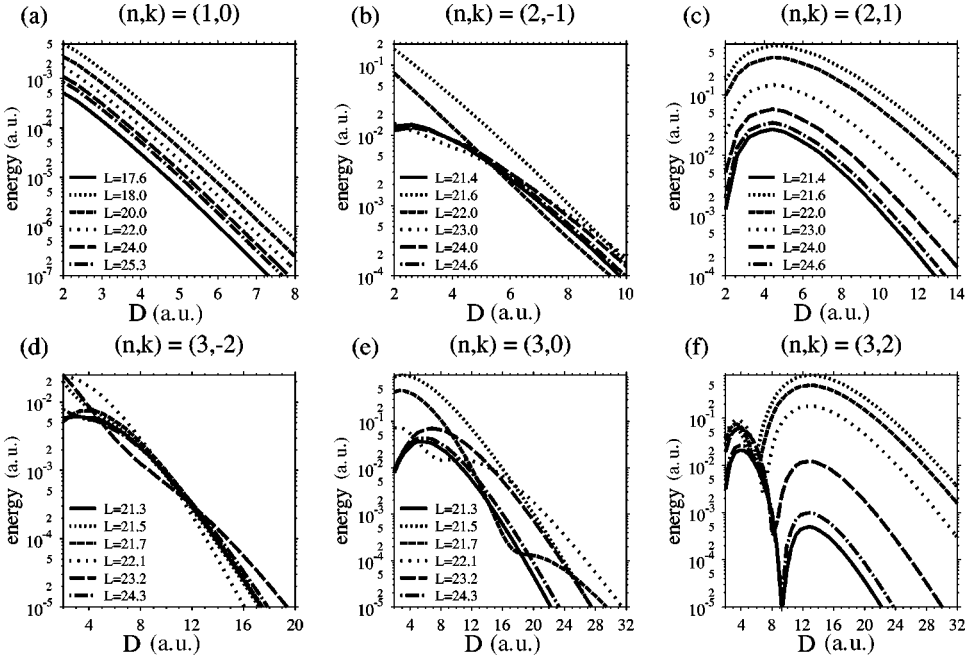

FIG. 6. Dependence of the level widths Γ_{nkm} on the atom-film distance D for a hydrogen atom in front of an Al(111) film, for the quantum numbers n,k,m of Fig. 4 and selected L values below and inside the intervals I_n defined in Eq. (14).

$=10^{-2}$ a.u. and in Fig. 8 for $v_z=10^{-4}$ a.u. The values chosen for the film thickness L are the same as those in Fig. 6.

With decreasing D, all curves in Figs. 7 and 8 (except those in plot (a) of Fig. 7; see below) drop from unity to zero in a fairly narrow D interval, so that it is meaningful to associate transition distances D_{nkm} (cf. end of Sec. II) with the different curves. The threshold effects observed in the L dependence of the level widths of Fig. 6 for $k=k_{\max}$ are reflected directly in the behavior of the transition distances in Figs. 7 and 8: the rapid rise of the level widths across the L thresholds corresponds to a drastic reduction of the time associated with the electronic transition, and hence to a much larger transition distance.

The transition distances in Figs. 7 and 8 exhibit a weak (near-logarithmic) dependence on the velocity component v_z, which reflects the near-exponential behavior of the level widths as a function of D. The velocity $v_z=10^{-2}$ a.u. chosen for the calculations of Fig. 7 appears to be a ''high'' velocity as the corresponding transition distances are [except for a few L-values at $(n,k)=(2,1)$ and $(3,2)$] smaller than the respective classical threshold distances for the superposition of the Jennings potential (1), the core image potential and the potential (7) [these distances are larger than the distances D_n introduced above by a factor 1.5]. In other words, the time elapsing until the atom reaches the classical threshold distance is too short for (classically forbidden) tunneling transitions to occur. The departure of two of the curves in plot (f) of Fig. 7 from the simple ''S'' shape can also be ascribed to

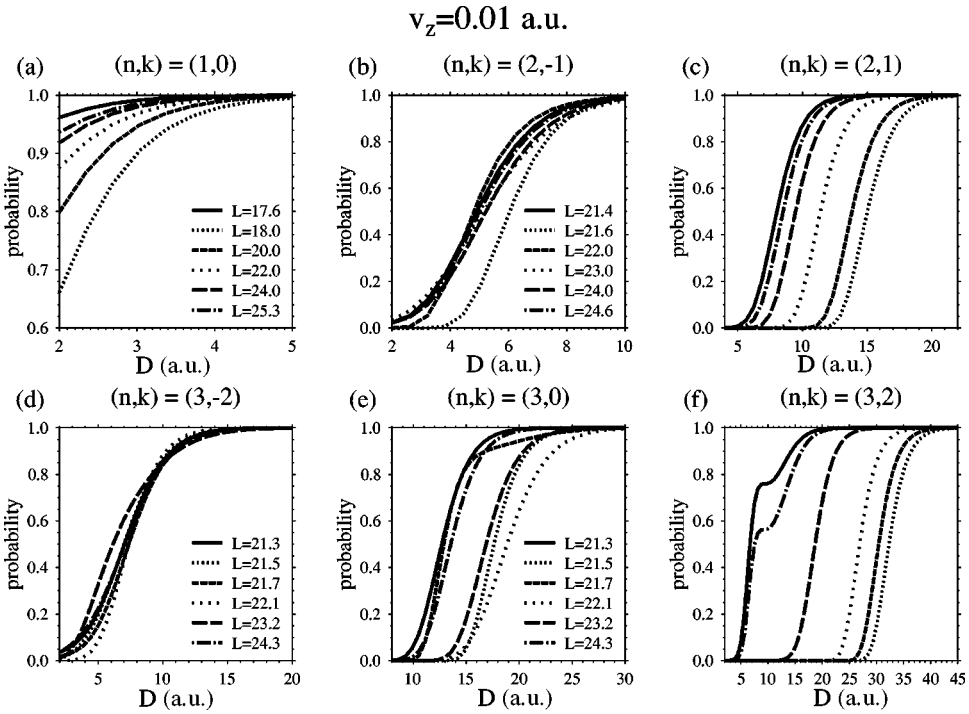

FIG. 7. Dependence of the occupation probabilities P_{nkm} [cf. Eq. (13)] on the atom-film distance D for the case of Fig. 6 and $v_z=10^{-2}$ a.u.

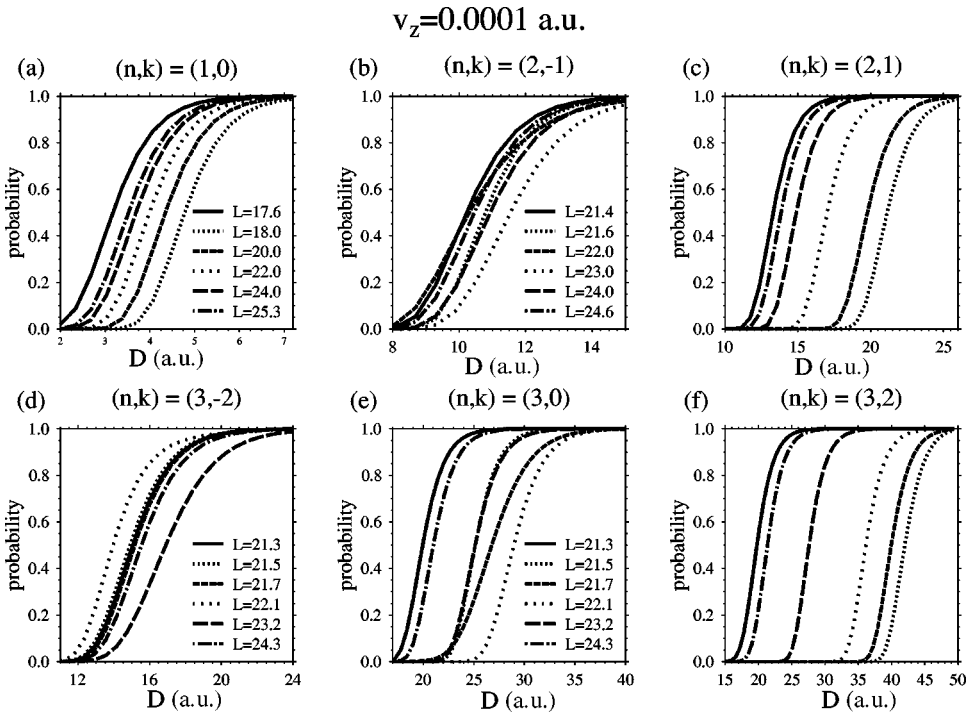

FIG. 8. Same as Fig. 7, for $v_z = 10^{-4}$ a.u.

the high (nonadiabatic) velocity: within the transition time, the atom enters a region close to the film where the D dependence of the level widths displays structure [cf. plot (f) of Fig. 6]. The velocity $v_z = 10^{-4}$ a.u. chosen for the calculations of Fig. 8, on the other hand, is low enough so that in most cases the transitions take place beyond the classical threshold distance, i.e., in the tunneling regime, and ''S''-shaped curves are found throughout for the D dependence of the probabilities.

The detailed L dependence of the transition distances D_{nkm} for the hydrogen $n = 1,2,3$ manifolds with $m = 0$, calculated in the intervals (14) for $v_z = 10^{-2}$ a.u. and $v_z = 10^{-4}$ a.u., is shown in Fig. 9 in a linear plot. The shapes of the curves bear a close resemblance to the shapes of the corresponding curves in the log-lin plots of the L dependence of the level widths in Fig. 5, in particular with regard to the pronounced threshold effects in the cases $k = k_{\max}$. The reason behind this resemblance is that the level widths behave near exponentially in the D ranges probed, with slopes depending only weakly on the film thickness L. For the examples of Fig. 9, the absolute magnitude of the threshold discontinuity in the transition distances for $k = k_{\max}$ is found to scale approximately with n^2, i.e., it scales in the same way as the atomic orbital radius and the classical threshold distance (the discontinuities read from Fig. 9 are in fact close to the absolute values of the threshold distance D_n for the steplike jellium potential). When averaged over the periodicity intervals of Fig. 9, the transition distances for fixed n exhibit

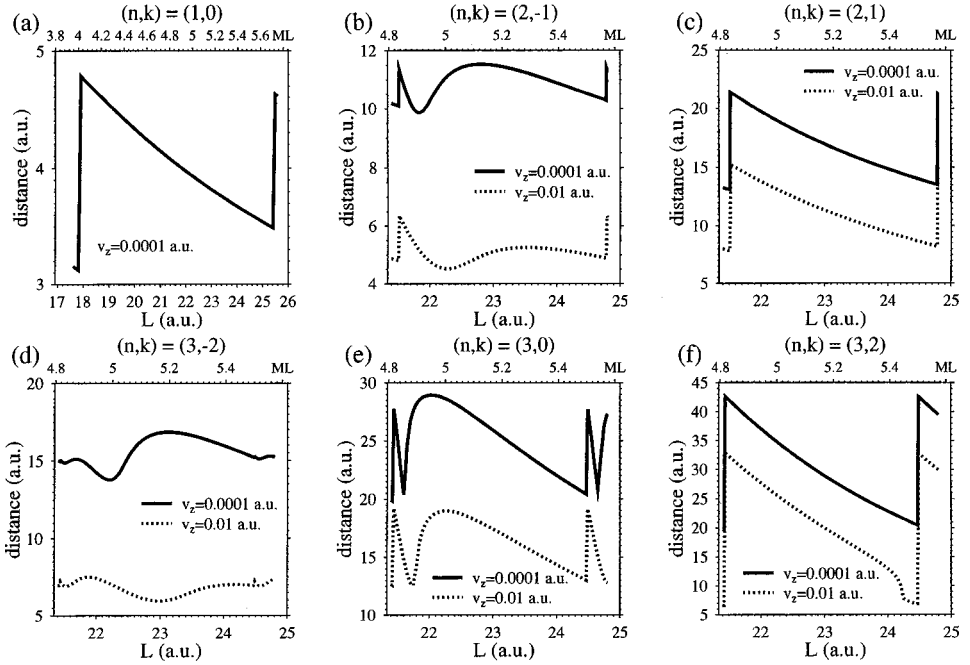

FIG. 9. Dependence of the transition distances D_{nkm} on the film thickness L for a hydrogen atom in front of an Al(111) film, evaluated over the intervals I_n defined in Eq. (14), for the quantum numbers n,k,m of Fig. 4 and $v_z = 10^{-2}$ a.u. and 10^{-4} a.u.

a change with the electric quantum number k that is equal to the change in the electric dipole moment $d=\frac{3}{2}nk$ of the Stark orbitals (note that we use atomic units). This feature appears to reflect a ''scaling'' for the widths of Stark orbitals in terms of the effective atom-surface distance $D^{\rm eff}=D-d$, similar to the scaling observed for the case of a semi-infinite metal target.[25]

The abrupt threshold discontinuities in the L dependence of the level widths calculated from Eq. (8), as well as in the transition distances derived therefrom, will clearly become somewhat shifted and blurred if the atomic level shift is taken into account in Eq. (8), i.e., if the energy ϵ_n is replaced with a D-dependent perturbed energy. However, for the examples to be discussed in Sec. V, the effect of the level shift on the discontinuities is expected to be small and hence can be disregarded in a qualitative discussion.

V. DISCUSSION

We now discuss some general trends exhibited by the results of Secs. III and IV and examine the possibility that features revealed by these results may be observed in suitably devised experiments.

The overall magnitude of the level widths resulting from averaging over the saw-tooth structures in Fig. 4 depends on the electric quantum number k in a way that reflects the orientation of the parabolic atomic orbitals with respect to the film plane: orbitals with maximum (minimum) k within an n manifold are preferentially oriented towards (away from) the film and hence have maximum (minimum) overlap with the film states and maximum (minimum) width. Owing to the increase of the density of film states with increasing L, the averaged level widths rise monotonically with L.

The gross structure of the L dependence of the widths in Fig. 4 is characterized by the periods and amplitudes of the saw-tooth patterns. The periods for the different atomic levels are determined solely by details of the film level diagram shown in Fig. 2 and are approximately proportional to the inverse of the level density and of the magnitude of the slope of the energy curves. In the examples of Fig. 4, the length of the periods increases from ≈ 3 a.u. for $n=3$ to ≈ 8 a.u. for $n=1$, i.e., the periods are associated with changes in the film thickness between one and two monolayers for Al(111). The amplitudes depend on details of the film level curves as well as on the atomic quantum numbers n and k. For $k=k_{\rm max}$, the amplitudes in Fig. 4 reflect, according to the discussion in Sec. III B, the true variation of the level width over one period. The rapid increase of this variation with increasing n can be traced to the behavior of the corresponding transition-matrix elements as a function of $k_\parallel$ (cf. Fig. 3). For electric quantum numbers $k<k_{\rm max}$, the curves in Fig. 4 are to be interpreted as averages over the detailed structure in one period. With this reservation, we conclude from Fig. 4 that for fixed n, the amplitudes decrease rapidly with decreasing k. Stated differently, the gross structure in the L dependence of the level widths becomes more and more pronounced when the overlap of the parabolic orbitals with film states gets larger.

The rapid modulations in the detailed structure of the L dependence of the level widths shown in Fig. 5 are associated (exactly as those in the $k_\parallel$-dependence of the transition-matrix elements for the semi-infinite case shown in Fig. 3) with the nodal structure of the atomic wave functions. The characteristic length of the modulations is of the order of 1 a.u. for the examples of Fig. 5 and is expected to be even smaller for larger n. It thus corresponds to changes in the film thickness on a submonolayer scale for Al(111).

The D dependence of the level widths at fixed L as shown in Fig. 6 exhibits features similar to those observed in the case of a semi-infinite metal target,[17,18] with details associated with the nodal structure of the atomic wave functions. Notably, with respect to its dependence on the electric quantum number k, the qualitative behavior of the detailed structure in the D dependence of the widths is reciprocal to that of the structure in the L dependence. Within the $n=3$ manifold, in particular, the number of extrema in the D dependence is seen to increase with increasing value of k (cf. Fig. 6), while the opposite is true for the L-dependence (cf. Fig. 5). This behavior appears to be related to the fact that the D dependence of the widths essentially samples properties of the atomic states in coordinate space, while the L-dependence samples momentum space properties. The reciprocal behavior may also be inferred from a detailed analysis of the $k_\parallel$ and D dependence of the transition-matrix element $W_{nlm,\vec{k}_\parallel i}(D)$ [cf. Eq. (12)], exploiting the explicit dependence of the atomic form factor $A_{nlm,\vec{k}_\parallel}$ on $k_\parallel$ and z as given by Eq. (A4).

As for the level widths, the gross structure of the calculated L dependence of the transition distances for the $n=1,2,3;m=0$ manifolds of hydrogen atoms interacting with an Al(111) film is characterized by periods in the range of one to two monolayers, while the modulations in the detailed structure are on the submonolayer scale. These features, along with the large threshold discontinuities in the transition distances for the states oriented towards the film, are to be considered when the possibility of an experimental verification of our results is discussed.

In principle, distances of individual electronic transitions taking place when an atom approaches a metallic target can be determined by studying resonance ionization of excited atoms (with the active electron occupying an atomic level lying above the Fermi level of the metal). For Rydberg atoms interacting with a semi-infinite metal, it has been suggested[26] that ionization distances may be inferred by measuring the ion yield as function of an applied external electric field, which serves to remove the ions from the interaction region. In order to obtain ''unperturbed'' ionization distances from the ion yields, a fairly complex theoretical analysis correcting for the effect of the external field is necessary.[27–29] Initial experiments using the technique of Ref. 26 have been deemed inconclusive.[27] However, experimental efforts continue.[30] Regarding the interaction of atoms with thin metallic films, the use of Rydberg atoms may be particularly tempting in view of the huge variation of the ionization distances with the film thickness, which are anticipated by extrapolating our results to large atomic quantum numbers.

Another promising way to observe features revealed by our calculations appears to be the study of resonance neutralization of *highly charged* ions. When a highly charged ion approaches a metal surface, electrons initially occupying metal states close to the Fermi level are transferred to the ion

in a sequence of individual resonant transitions at different distances into ionic states with different principal quantum numbers (corresponding to different effective core charges of the ion), leading ultimately to the formation of a highly excited, ''hollow'' atom.[1,31] The set of individual transition distances determines the kinetic energy gain of the ion due to the image charge interaction,[32,3] which can be measured in grazing-incidence scattering experiments. As for surfaces, for thin metallic films electrons are resonantly transferred to the ion from initial states close to the Fermi level, i.e., transferred to ionic states at a fixed energy. As a function of L, the Fermi level varies only weakly[8] over one period of the gross structure. The position of the thresholds in the L dependence of the transition distances are thus expected to be largely independent of the specific transition (cf. Fig. 2). Loosely speaking, the different distances then vary ''in-phase'' as a function of L. As L increases, the transition distances corresponding to ionic orbitals with the maximum electric quantum number $k_{\max}$, which are the largest distances within an n manifold (cf. Fig. 9), will collectively rise when a threshold is passed, with a subsequent collective decrease. This may give rise to substantial variations in the effect of the image charge interaction and in the associated kinetic-energy gain of the ion.

For the actual observation of effects of the kind revealed by our calculations, it is prerequisite, of course, that thin metallic films can be grown with sufficient control of the thickness. For gross structure effects to become discernible, control at the one-monolayer level is required. For the description of variations of film properties at the submonolayer level, the use of a potential that is translationally invariant in the film plane is questionable. The direct experimental observation of the detailed structure found in our calculations may not be possible. However, experimental evidence for the calculated detailed structure in the L dependence may be found indirectly due to the fact that the L-periodicity intervals do not coincide with the spacing between film layers.

VI. SUMMARY AND CONCLUSIONS

We have theoretically studied the broadening of atomic levels near thin-metallic films. Adopting the fixed-atom approximation and employing hydrogenic states in parabolic representation, we have evaluated first-order level widths for the $n=1,2,3; m=0$ manifolds of a hydrogen atom interacting with an Al(111) film. The calculations were facilitated by using an efficient expression for the relevant transition-matrix elements in terms of analytically given atomic form factors. Pronounced structure is found in the dependence on the film thickness of the widths, as well as of the atomic occupation probabilities and transition distances derived therefrom. The gross features of this (near-periodic) structure essentially image the quantized energy level spectrum arising from the electron confinement in the growth direction of the film. Finer details of the structure can be understood by disclosing analogies between the thickness dependence of the level widths for thin films and the dependence of the transition-matrix elements on the wave vector component parallel to the surface for semi-infinite metal targets.

The variations of the calculated transition distances with film thickness are so large that experimentally observable effects are conceivable. Among the possible ways towards an experimental verification of our results, resonance neutralization of highly charged ions near thin-metallic films appears to be promising. We have argued that in resonance neutralization, the different transition distances corresponding to different effective charges of the ion may vary ''in-phase'' as a function of the film thickness. This may give rise to sizeable variations in the energy gain of the ions caused by the image charge interaction.

In future investigations, we plan to calculate the full electronic selfenergy of hydrogenic atoms interacting with thin metallic films. As in our study of the self energy for semi-infinite metals,[14] we may consider separately the contributions of the various couplings among the atomic basis states and analyze, in particular, the interplay between direct couplings and indirect couplings via metal states. Adiabatic resonance states generated from the self-energy for thin films may serve as basis states in time-dependent close-coupling calculations for the electronic dynamics in atom-film interactions, in close analogy to the semi-infinite case.[29,33] The extension of the present calculations to the case of layered structures composed of arbitrary sequences of metals, semiconductors, and insulators, and involving arbitrary z-profiles, is straightforward. Possible applications of calculations of this kind may be found, e.g., in the analysis of electron transfer in ion desorption processes.[34,35] These processes have considerable practical relevance in surface and thin-film analytical methods.

ACKNOWLEDGMENT

This work was supported by the National Science Foundation under Grant No. PHY-9604872 and by the Division of Chemical Sciences, Basic Energy Sciences, Office of Energy Research, and U.S. Department of Energy. One of us (U.T.) acknowledges the hospitality of the Institute for Theoretical Atomic and Molecular Physics at Harvard University and the Smithsonian Observatory.

APPENDIX A: MATRIX ELEMENTS IN TERMS OF ATOMIC FORM FACTORS

We consider matrix elements of the general form

$$\mathcal{M}^{(j)}_{nlm,\vec{k}_\parallel} = \int d\vec{r}\, \psi^*_{nlm}(\vec{r}) f_j(\vec{r}) \exp(i\vec{k}_\parallel \cdot \vec{r}_\parallel) g(z) \quad \text{(A1)}$$

with hydrogenic wave functions $\psi_{nlm}(\vec{r})$ in spherical representation. The function $f_j(\vec{r})$ is either unity ($j=1$), or equal to the Coulomb potential $V_C(\vec{r})$ defining the hydrogenic functions ($j=2$), and $g(z)$ is an arbitrary function (note that $z=0$ is chosen here to correspond to the atomic center). The class of matrix elements (A1) comprises all individual matrix elements of the initial-channel perturbation (assuming a one-dimensional approximation to the core image potential) as well as the overlap matrix elements appearing in the full self energy of a hydrogenic atomic system in front of a jellium metal surface[14] or a layered structure (in particular, thin film) with arbitrary z profile.

Introducing the momentum space representation $F^{(j)}_{nlm}(\vec{q})$ of the product $f_j(\vec{r})\psi_{nlm}(\vec{r})$,[23] we can immediately perform the integration over $\vec{r}_\parallel$ and write the matrix elements (A1) as

$$\mathcal{M}^{(j)}_{nlm,\vec{k}_\parallel} = \int_{-\infty}^{\infty} dz\, g(z) A^{(j)}_{nlm,\vec{k}_\parallel}(z), \tag{A2}$$

where the function

$$A^{(j)}_{nlm,\vec{k}_\parallel}(z) = \int_{-\infty}^{\infty} dq_z\, F^{(j)}_{nlm}(\vec{k}_\parallel; q_z) \exp(iq_z z) \tag{A3}$$

is referred to as the ''atomic form factor.'' The integral over q_z is closely related to integrals appearing in Ref. 23 and can be evaluated in closed form by using complex contour integration. (Note that in Ref. 23, the q_z integration is performed *after* the z integration over the wave functions for a steplike jellium potential and has been done analytically. The integrands in the q_z-integrals of Ref. 23 therefore contain, in comparison with the present case, an additional pole term.) Explicitly, we have

$$A^{(j)}_{nlm,\vec{k}_\parallel}(z) = (-1)^{l+m}(2\pi)^{3/2} \frac{\exp(-k_+ z)}{2^{n-j+2} k_+^{2(n-j+1)+1}} \times \mathcal{S}_j^{(n-j+2)}(n-j+1; k_+; z), \tag{A4}$$

for $z \geq 0$, and

$$A^{(j)}_{nlm,\vec{k}_\parallel}(-z) = (-1)^{l+m} A^{(j)}_{nlm,\vec{k}_\parallel}(z). \tag{A5}$$

In Eq. (A4), the parameter k_+ is defined as $k_+ = (k_\parallel^2 + (Z/n)^2)^{1/2}$, and $\mathcal{S}_j^{(n-j+2)}(n-j+1; k_+; z)$ is a polynomial of degree $n-j+1$ in z whose explicit form is given in Ref. 23 (note that the dependence of $\mathcal{S}$ on the quantum numbers l and m is not explicitly indicated).

By means of the symmetry property (A5) for the atomic form factor, the integral (A2) can be rewritten as

$$\mathcal{M}^{(j)}_{nlm,\vec{k}_\parallel} = \int_0^{\infty} dz \{g(z) + (-1)^{l+m} g(-z)\} A^{(j)}_{nlm,\vec{k}_\parallel}(z). \tag{A6}$$

Specializing to the case of interest for the present work, we retrieve from Eq. (A6) the form (12) for the transition matrix elements $W_{nlm,\vec{k}_\parallel i}$ by setting $j=2$ and $g(z) = \Theta(z+D)\phi_i(z+\Delta)$, where $\Delta \equiv L/2 + D$, and by changing the integration variable from z to ζ [note that the superscript $j=2$ is omitted in the form factor in Eq. (12)].

*Present address: SAP, Neurottstr. 16, D-69190 Walldorf, Germany.

[1] A. Arnau, F. Aumayr, P.M. Echenique, M. Grether, W. Heiland, J. Limburg, R. Morgenstern, P. Roncin, S. Schippers, R. Schuch, N. Stolterfoht, P. Varga, T.J.M. Zouros, and HP. Winter, Surf. Sci. Rep. **27,** 113 (1997).

[2] L. Hägg, C.O. Reinhold, and J. Burgdörfer, Phys. Rev. A **55**, 2097 (1997).

[3] J.J. Ducrée, F. Casali, and U. Thumm, Phys. Rev. A **57**, 338 (1998).

[4] P. Nordlander and J.P. Modisette, Nucl. Instrum. Methods Phys. Res. B **125**, 305 (1997).

[5] J.P. Gauyacq and A.G. Borisov, J. Phys.: Condens. Matter **10**, 6585 (1998).

[6] H. Khemliche, T. Schlathölter, R. Hoekstra, R. Morgenstern, and S. Schippers, Phys. Rev. Lett. **81**, 1219 (1998).

[7] A.G. Borisov and H. Winter, Nucl. Instrum. Methods Phys. Res. B **115**, 142 (1996).

[8] A.G. Borisov and H. Winter, Z. Phys. D **37,** 263 (1996).

[9] G. Bastard, *Wave Mechanics Applied to Semiconductor Heterostructures* (Les Éditions de Physique, Les Ulis, 1996).

[10] Q. Yan, J. Burgdörfer, and F.W. Meyer, Phys. Rev. B **56,** 1589 (1997).

[11] R. Pfandzelter, T. Igel, and H. Winter, Surf. Sci. **389,** 317 (1997).

[12] T. Igel, R. Pfandzelter, and H. Winter, Surf. Sci. **405,** 182 (1998).

[13] J. Burgdörfer, E. Kupfer, and H. Gabriel, Phys. Rev. A **35,** 4963 (1987).

[14] P. Kürpick, U. Thumm, and U. Wille, Phys. Rev. A **56,** 543 (1997).

[15] P. Kürpick and U. Thumm, Phys. Rev. A **58**, 2174 (1998).

[16] P.J. Jennings, R.O. Jones, and M. Weinert, Phys. Rev. B **37**, 6113 (1988).

[17] U. Wille, Nucl. Instrum. Methods Phys. Res. B **125**, 310 (1997).

[18] A.G. Borisov and U. Wille, Surf. Sci. **338**, L875 (1995).

[19] A.G. Borisov and U. Wille, Nucl. Instrum. Methods Phys. Res. B **115,** 137 (1996).

[20] U. Wille, Phys. Rev. B **50,** 1888 (1994).

[21] U. Thumm and J.S. Briggs, Nucl. Instrum. Methods Phys. Res. B **43,** 471 (1989).

[22] D. Park, Z. Phys. **159**, 155 (1960).

[23] U. Wille, Phys. Rev. A **45,** 3004 (1992).

[24] U. Wille, Surf. Sci. **307-309**, 874 (1994).

[25] A.G. Borisov, R. Zimny, D. Teillet-Billy, and J.P. Gauyacq, Phys. Rev. A **53**, 2457 (1996).

[26] D.F. Gray, Z. Zheng, K.A. Smith, and F.B. Dunning, Phys. Rev. A **38,** 1601 (1988).

[27] P. Nordlander and F.B. Dunning, Phys. Rev. B **53**, 8083 (1996).

[28] P. Nordlander and F.B. Dunning, Nucl. Instrum. Methods Phys. Res. B **125,** 300 (1997).

[29] P. Kürpick, U. Thumm, and U. Wille, Phys. Rev. A **57**, 1920 (1998).

[30] F.B. Dunning (private communication).

[31] U. Thumm, Phys. Rev. A **55**, 479 (1997); Comments At. Mol. Phys. **34,** 119 (1999).

[32] H. Winter, J. Phys.: Condens. Matter **8,** 10149 (1996).

[33] P. Kürpick, U. Thumm, and U. Wille, Nucl. Instrum. Methods Phys. Res. B **125**, 273 (1997).

[34] M.B. Raschke and T.E. Madey, Phys. Rev. B **58,** 15 832 (1998).

[35] Q.-B. Lu, Z. Ma, and T.E. Madey, Phys. Rev. B **58,** 164 46 (1998).